Wind Lidar for Atmospheric Research

30

Oliver Reitebuch

Abstract

Wind lidars use the optical Doppler effect to measure the atmospheric wind with high spatial and temporal resolution. This offers a wide range of applications from aircraft wake vortex detection and characterization to measurement of turbulent quantities like fluxes to resolving small and mesoscale atmospheric flows, and even global wind profiling from space in the future. Principles of wind lidars including two complementary techniques and applications for atmospheric research are discussed.

30.1 Introduction

Wind observations with *lidar* (light detection and ranging) systems were used by scientists from the DLR Institute of Atmospheric Physics (IPA) to study atmospheric flow on a large variety of scales: from atmospheric turbulence to aircraft wake vortices or flows around wind turbines to mesoscale atmospheric flows, e.g., within mountain valleys or land-sea breeze circulation, to large scale flows like jet streams or typhoon outflows. Different types of wind lidars allow measurements in different altitude regions of the atmosphere from the atmospheric boundary layer with high aerosol content to the upper troposphere, stratosphere and even mesosphere with molecules as backscattering targets. Optical *remote sensing* with lidar

O. Reitebuch (✉)
DLR, Institute of Atmospheric Physics (IPA), Münchner Straße 20,
82234 Oberpfaffenhofen, Germany
e-mail: Oliver.Reitebuch@dlr.de

U. Schumann (ed.), *Atmospheric Physics*, Research Topics in Aerospace,
DOI: 10.1007/978-3-642-30183-4_30,

is a very powerful method for measuring the atmospheric wind vector. It is possible to measure the horizontal wind vector as well as the vertical wind component with different viewing geometries. Wind lidars are operated from ground, balloon, ship, or aircraft and will be deployed on satellites in the future.

The movement of the air is described by the wind vector $\mathbf{V} = (U, V, W)$, which is composed of three components, in contrast to most other atmospheric variables such as temperature, humidity or pressure, which are scalar parameters. Usually the wind vector is described by a vertical component W (up and down along the axis of Earth gravity, positive for an updraft wind) and two horizontal components U, V. The horizontal wind vector ("velocity") can be either described by the magnitude of the vector V_h ["wind speed"; $V_h = \sqrt{(U^2 + V^2)}$] and by the wind direction θ (angle between the horizontal wind vector and north; $\theta = \arctan(U/V)$; $\theta = 0°$ for northerly wind, wind from north towards south, $\theta = 90°$ for easterly wind, wind from east to west), or it is decomposed into the two components along the west-east axis U (zonal wind component, positive if wind is blowing from west towards east, which is a westerly wind) and along the south-north axis V (meridional wind component, positive if wind is blowing from south to north, which is a southerly wind).

30.2 Principle of Wind Lidar Methods

Most wind lidars rely on the use of the optical Doppler effect to measure wind speed, thus they are usually named *Doppler wind lidars* (DWL). Nevertheless, it should be mentioned that correlation techniques from two successive images (similar to the derivation of cloud-drift winds) or from two different range measurements (e.g., used by the police for speed measurements) are also used for specific applications to determine wind speed.

DWL instruments determine the component of the wind vector which is projected onto the *laser* beam propagation direction—the so called *line-of-sight* (LOS) with its unit pointing vector **D**. The vector **D** can be described by the angle α, between the LOS direction and the zenith (for ground DWL) or nadir (for airborne and space-borne DWL) and the azimuth angle β between the LOS direction and the north direction in the horizontal plane. This LOS wind speed component v_{LOS}, or v for short, (in units of m/s) is obtained by the projection of the wind vector **V** on the LOS direction **D**:

$$v_{LOS} = \vec{D} \cdot \vec{V} = \sin(\alpha) \cdot \sin(\beta) \cdot U + \sin(\alpha) \cdot \cos(\beta) \cdot V + \cos(\alpha) \cdot W$$
$$v_{LOS} = \sin(\alpha) \cdot V_{h,||} + \cos(\alpha) \cdot W$$

When only the horizontal wind speed $V_{h,||}$ in the plane of the LOS direction is considered, then v_{LOS} is determined by the off-nadir or off-zenith angle α (as indicated in Fig. 30.2). Thus for a measurement of the vertical wind W, the laser beam has to be directed vertically ($\alpha = 0°$), whereas for the horizontal wind

vector, a minimum of two preferably orthogonal LOS directions tilted towards the horizontal plane with an angle of α are used. If the LOS direction and the wind vector are perpendicular, then no LOS wind speed is observed. Depending on the pointing direction **D** towards zenith from ground or nadir from space, the sign of the above equations has to be adapted to be consistent with the meteorological definition of the sign for U, V, W and the sign definition for v_{LOS} in the *Doppler shift* equations below.

A DWL determines the wind speed of the air by using the collective motion of a large number of aerosols, cloud particles and molecules within the air volume as tracers. Different methods are applied for using aerosol and cloud particles as tracers with a *coherent detection DWL* and molecules as tracers with a *direct-detection DWL* (which is also called "incoherent" detection DWL). A direct-detection lidar relies on the measurement of the signal intensity or number of photons, whereas a coherent lidar measures in addition the phase and frequency of the backscattered signal. Overviews of DWL principles, techniques and applications can be found in Vaughan et al. (1996), Werner (2004), and Henderson et al. (2005).

30.2.1 The Doppler Effect

Most wind lidars rely on the Doppler effect, which was first described by the Austrian physicist Christian Doppler in 1842. The Doppler effect can be observed for *acoustic waves*, which is used in remote sensing with a Doppler sodar (sonic detection and ranging), for electromagnetic waves, which is used for Doppler *radar* (radio detection and ranging), and for lidar. It describes the change in *frequency* (or *wavelength*) that is present when the source of the wave and the observer are in relative motion to each other. The correspondence of the frequency f_0 and the wavelength λ_0 of an electromagnetic wave is obtained using the *speed of light* c ($c = 2.9979 \times 10^8$ m/s):

$$f_0 = \frac{c}{\lambda_0}$$

The change in frequency Δf or wavelength $\Delta\lambda$ is referred to as the Doppler shift and can be positive or negative, depending on the direction of the relative movement. For the case that a laser is emitting a light wave with frequency f_0, an observer moving with velocity v would detect the frequency f_1 with:

$$f_1 = f_0 \cdot \left(1 + \frac{v}{c}\right)$$

The velocity $v = v_{LOS}$ describes the movement of source and observer relative to each other. The Doppler frequency shift Δf or wavelength shift $\Delta\lambda$ is obtained from:

Table 30.1 Doppler shift for a line-of-sight speed of 1 m/s for typical wavelengths of a DWL

λ_0/μm	f_0/THz	$\Delta\lambda$/fm	Δf/MHz
0.355	845	2.37	5.63
2.02	148	13.5	0.987
10.6	28.3	70.7	0.189

$$\Delta f = f_1 - f_0 = f_0 \cdot \frac{\mathrm{v}}{c}$$
$$\Delta\lambda = \lambda_1 - \lambda_0 = -\lambda_0 \cdot \frac{\mathrm{v}}{c}$$

The Doppler wavelength shift $\Delta\lambda$ is positive (called the "red shift", because the wavelength is shifted towards larger wavelengths λ_1, which are towards red spectral colors) if the velocity v is negative and the distance between source and observer increases. If the velocity v is positive, then the observer is moving towards the source, and the wavelength is decreasing ("blue shift") and the frequency increasing.

For a Doppler lidar (but also for Doppler radar and sodar) the Doppler effect occurs two times. First, when the light wave from the emitting laser source with a frequency of f_0 is perceived by the moving, scattering particle (aerosol, cloud, molecule) and thus is exposed to a light wave of frequency f_1; the second Doppler effect occurs when the moving particle re-emits the scattered wave with frequency f_1, which is perceived by the lidar receiver as a wave with frequency f_2:

$$f_2 = f_1 \cdot \left(1 + \frac{\mathrm{v}}{c}\right) = f_0 \cdot \left(1 + \frac{\mathrm{v}}{c}\right)^2 = f_0 \cdot \left(1 + 2 \cdot \frac{\mathrm{v}}{c} + \frac{\mathrm{v}^2}{c^2}\right) \approx f_0 \cdot \left(1 + 2 \cdot \frac{\mathrm{v}}{c}\right)$$

The term v^2/c^2 can be neglected, as it is a factor of 10^{-7}–10^{-8} smaller than the term v/c for usual atmospheric wind speeds v compared to the speed of light c. The Doppler frequency and wavelength shift can be finally written as:

$$\Delta f = f_2 - f_0 = 2 \cdot f_0 \cdot \frac{\mathrm{v}}{c}$$
$$\Delta\lambda = \lambda_2 - \lambda_0 = -2 \cdot \lambda_0 \cdot \frac{\mathrm{v}}{c}$$

The relative Doppler shift expressed as $\Delta f/f_0$ or $\Delta\lambda/\lambda_0$ is in the order of 10^{-7}–10^{-8} for electromagnetic waves and typical atmospheric wind speeds. It is very demanding to detect such small changes in the frequency of a light wave, which sets high challenges for the laser sources and optical receivers used for a DWL. For illustration, the Doppler shifts for typical wavelengths of a DWL are provided in Table 30.1. A 1 m/s LOS wind speed would change the wavelength of a DWL from 2.02 to 2.0200000135 μm, by only 13.5 fm (1 fm = 10^{-15} m).

30.2.2 Spectral Line Shape from Molecular and Particle Backscatter

The collective, mean movement of all molecules, aerosol, and cloud particles within a certain atmospheric volume is referred to as wind. This is superimposed by the random, thermal motion of the molecules and particles ("Brownian motion") and causes so-called *Doppler broadening*. This motion can be described by the *Maxwell–Boltzmann velocity distribution*, which is dependent on the atmospheric temperature T and the mass m of a single molecule (or particle). The mean velocity of the air molecules (mixture of gases with mean mass $m = 4.79 \times 10^{-26}$ kg) is quite high with a value of 459 m/s for a temperature of 15 °C. If only one component in the LOS direction of the velocity distribution is considered, then it can be described by a Gaussian distribution with a standard deviation in velocity space σ_v or wavelength space σ_λ after applying the Doppler shift equation:

$$\sigma_v = \sqrt{\frac{k \cdot T}{m}} \qquad \sigma_\lambda = \frac{2 \cdot \lambda_0}{c} \sqrt{\frac{k \cdot T}{m}}$$

with Boltzmann constant k ($k = 1.38 \times 10^{-23}$ J/K). The Gaussian approximation is only valid for dilute gases. For typical atmospheric densities an additional *Brillouin scattering* effect on moving pressure fluctuations has to be considered, which is described by Rayleigh-Brillouin scattering (Witschas et al. 2010). The Gaussian velocity distribution is quite broad for air molecules with $\sigma_v = 288$ m/s and a *full-width at half-maximum* (FWHM) of 678 m/s for 15 °C. (FWHM $= 2\sqrt{(2 \ln(2))} = 2.355$ for a Gaussian distribution with unit standard deviation.) For aerosol and cloud particles the width of the velocity distribution is several orders of magnitude smaller due to the larger mass of aerosols and cloud particles. The assumptions of typical particle radii of 0.1–1 μm, which are of sizes relevant for Mie scattering at laser wavelengths, and of spherical water particles (density of 10^3 kg/m^3) lead to typical masses of 4.2×10^{-18}–4.2×10^{-15} kg. Thus Doppler broadening is a factor of 10^4–10^6 smaller for aerosol particles compared to molecules.

The mean of the Gaussian velocity distribution is given by the mean, collective movement of all molecules, which is referred to as LOS wind speed. For the case that a laser emits a wavelength λ_0, the backscattered light from molecules is spectrally broadly distributed, which is illustrated in Fig. 30.1, where the distribution of Doppler shifts is shown for a typical DWL wavelength of 355 nm. A broad bandwidth spectrum is obtained from molecules, whereas a narrow bandwidth spectrum is obtained from aerosol and cloud particles. In the case of a mean wind speed of the air volume, both the aerosol and the molecular spectrum are shifted in parallel along the wavelength axis.

The measurement of the wind speed is directly related to the measurement of the mean (or first moment) of the velocity or Doppler wavelength shift distribution. Either the broad bandwidth molecular backscatter return or the narrow

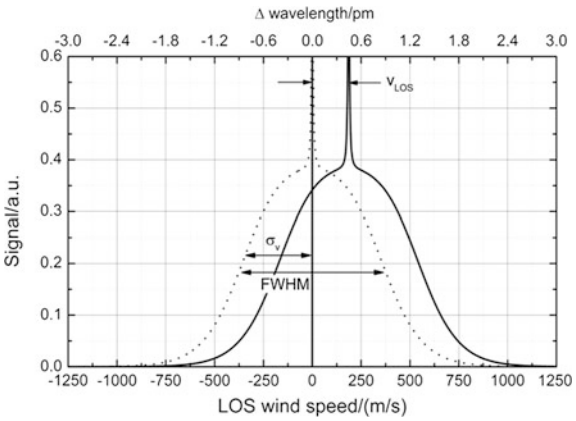

Fig. 30.1 Spectral distribution of LOS wind speed in m/s of broad bandwidth molecular and small bandwidth aerosol signal in arbitrary units (a.u.); corresponding Doppler wavelength shifts in pm for an emitted wavelength of $\lambda_0 = 355$ nm (1 pm equivalent to 422 m/s), standard deviation σ_v and FWHM are indicated; one spectrum (*dotted lines*) is shown for a mean LOS wind speed of 0 m/s, while the other spectrum (*bold line*) is shown for 180 m/s LOS wind speed (equivalent to a Doppler shift of 0.44 pm)

bandwidth aerosol backscatter return is used for wind determination. Although both techniques differ fundamentally in their technical realization (see next sections), the fundamental, theoretical limit of the minimum random error is given by the spectral distribution. This theoretical, statistical limit of the random error ε_v for the wind speed estimation only depends on the spectral width σ_v and the number of backscattered photons N_{ph} in the case of pure Poisson distributed photon noise:

$$\varepsilon_v = \frac{\sigma_v}{\sqrt{N_{photons}}} = \frac{\sigma_v}{\sqrt{N_{pulses} \cdot N_{photons/pulse}}}$$

The spectral width of the aerosol backscatter is dominated by the spectral width of the emitted laser pulse, due to the negligible Doppler broadening of the aerosol. Typically, this laser width is a factor of 100 smaller than the width of the broadband Rayleigh spectrum. Thus a factor of 10^4 more photons are needed to obtain the same random error if the Rayleigh spectrum is used for wind measurement. This can be achieved by averaging the backscattered signal from a number of laser pulses N_{pulse} and by increasing the detected number of photons per pulse $N_{photons/pulse}$, e.g., by higher laser pulse energies.

30.3 Wind Lidar Methods

IPA is one of few institutes worldwide where both DWL methods—namely coherent and direct-detection—are developed and operated. Some key parameters of airborne DWL at IPA are shown in Table 30.2 and are further discussed in the

Table 30.2 Key parameters of airborne Doppler wind lidar (DWL) at DLR

	Wind infrared Doppler lidar WIND	2-μm DWL	ALADIN airborne demonstrator A2D
Developer	DLR, CNRS, CNES, Meteo-France	DLR, Lockheed Martin Coherent Technologies	DLR, EADS-Astrium
Maiden flight	1999	2001	2005
Major campaigns	MAP 1999 (Alps) ESCOMPTE 2001 (France) AMMA 2006 (West Africa)	VERTIKATOR 2002 (Alps) A-TReC 2003 (Iceland) T-PARC 2008 (Japan) several aircraft wake vortex campaigns, e.g. A380 Eyjafjalla volcanic ash 2010 (Europe, Iceland)	Aeolus pre-launch validation 2007, 2008, 2009 (central Europe, Iceland)
Lidar principle	Coherent, heterodyne detection	Coherent, heterodyne detection	Direct-detection with double-edge and fringe imaging technique
Atmospheric backscatter	Aerosol and cloud particles	Aerosol and cloud particles	Molecules, aerosol and cloud particles
Laser type and wavelength	CO_2 gas laser 10.6 μm	Solid-state Tm:LuAG 2.02254 μm	Solid-state Nd:YAG 354.9 nm
Laser energy, repetition rate, pulse length	100–200 mJ 10 Hz 2–3 μs	1–2 mJ 500 Hz 400 ns (FWHM)	50–60 mJ 50 Hz 25 ns (FWHM)
Telescope Ø (cm)	20	10.8	20
Scanner	Conical scan with 30°	Conical scan with 20°, arbitrary scan patterns with double wedge	No scanner, only fixed LOS under 20° slant angle
Vertical resolution (m)	250	100	250
Power-aperture product mean ($mW \cdot m^2$)	47	7	86
Precision of wind observation	0.5–1.5 m/s horizontal wind speed	0.3–1.0 m/s horizontal wind speed	1–2 m/s LOS wind speed

next section. All were deployed on the DLR Falcon aircraft and used for numerous atmospheric and validation campaigns. Table 30.3 provides a comparative overview of coherent and direct-detection wind lidar. Coherent DWL usually operates in the eye-safe, infrared region of the spectrum with wavelengths of 1.5–1.6, 2 and 10 μm, whereas direct-detection DWL uses ultraviolet (355 nm), visible (532 nm) or near-infrared (1 064 nm) wavelengths. Coherent DWL are used for applications

Table 30.3 Comparative overview of different wind lidar techniques

	Coherent detection	Direct-detection
Wavelengths and lasers	CO_2 gas lasers 10.6 μm Tm:LuAG or Tm,Ho:YAG at 2 μm Er-doped fiber at 1.5–1.6 μm	Nd:YAG at 1 064 nm, frequency-doubled at 532 nm, and -tripled at 355 nm
Atmospheric backscatter	Aerosol and cloud particles narrow bandwidth line shape	Molecules with Rayleigh-Brillouin lineshape (broad bandwidth), aerosol and cloud return
Receiver	Mainly heterodyne detection some earlier systems used homodyne detection	(a) filter techniques, e.g., double edge or iodine filter (b) fringe imaging, e.g., Fizeau (c) two-beam interferometer, e.g., Mach–Zehnder
Dominating noise sources	Photon noise of local oscillator, speckle noise, atmospheric turbulence	Solar background light and signal photon noise
Calibration	No calibration needed, as relation between Doppler frequency shift and detected signal is obtained by Fourier transformation.	Calibration needed to obtain relationship between Doppler frequency shift and detected signal
Need for additional parameters	No additional parameters needed for wind retrieval	Atmospheric temperature and pressure needed for correction of retrieved wind from molecular backscatter
Technology readiness	Systems commercially available	Research systems, satellite lidar under development
Main applications	Need for high precision and high temporal resolution, aircraft wake vortex, turbulence, wind turbines, boundary layer winds, vertical wind speed, and turbulent fluxes	Wind sensing for higher altitudes of upper troposphere, stratosphere and mesosphere

where sufficient aerosol backscatter is present, e.g., for atmospheric boundary layer winds, whereas direct-detection DWL is the system of choice for higher altitudes up to the mesosphere. Coherent DWL are commercially available today, can be very compact and reliable, and high temporal resolution and high precision can be achieved, which even allows the determination of vertical winds, turbulent quantities, or aircraft wake vortices. Direct-detection DWL using molecular backscatter are the systems of choice for wind measurements in the upper troposphere, stratosphere and even up to the mesosphere.

30.3.1 Coherent Doppler Wind Lidar

The coherent DWL is the most common system concept today and is available as a reliable and easy to operate (“turn-key”) instrument from commercial companies. A coherent DWL is purely using the narrow bandwidth aerosol and cloud particle

backscatter return. Its principle relies on the optical mixing of two optical beams—one returned from the atmosphere and one from an instrumental internal source—and detection of the optical beat signal. Coherence is a characteristic of an electromagnetic wave which permits *interference* and is related to the *wave phase*. Waves radiating with a fixed relationship between their phases are coherent, which is the case for laser emissions, whether cw or pulsed. In contrast radiation from a light bulb is not coherent, because of the spontaneous, thermal generation of light waves with random relation between their phases. In principle, every type of lidar uses coherent emission with a laser source. A specific type of DWL is called coherent, because it uses in addition a coherent laser in the optical receiver and detection part of the instrument. The coherent DWL makes use of an additional cw laser source (called "local oscillator") and the coherence of the backscatter signal from the atmosphere to obtain a beat frequency signal from the interfering waves during optical mixing.

The Doppler frequency is determined by mixing two optical beams on an optical element. Here, the atmospheric signal $E_s(t)$ with its frequency $f_S = f_2 = f_0 + \Delta f$ and phase φ_S is optically mixed with the cw laser beam of the local oscillator $E_{LO}(t)$ with frequency f_{LO}. Both electrical field vectors of the light beams $E_s(t)$ and $E_{LO}(t)$ are summed up to $E_D(t)$, where the overbar denotes a temporal average in the following equations.

$$E_S(t) = \bar{E}_S \cdot \cos(2\pi \cdot f_s \cdot t + \varphi_S)$$
$$E_{LO}(t) = \bar{E}_{LO} \cdot \cos(2\pi \cdot f_{LO} \cdot t)$$
$$E_D(t) = E_S(t) + E_{LO}(t) = \bar{E}_S \cdot \cos(2\pi \cdot f_s \cdot t + \varphi_S) + \bar{E}_{LO} \cdot \cos(2\pi \cdot f_{LO} \cdot t)$$

The resulting beam with its electrical field $E_D(t)$ is directed to a detector which is sensitive to light intensities proportional to $|E_D(t)|^2$. As the detector current $I_D(t)$ cannot follow the optical frequencies with THz variations (second eq. below, last term) because those are much higher than the bandwidth of the detector, only the time-averaged signal of $|E_D(t)|^2$ is detected:

$$I_D(t) \propto \overline{|E_D(t)|^2}$$
$$I_D(t) \propto \tfrac{1}{2}\bar{E}_S^2 + \tfrac{1}{2}\bar{E}_{LO}^2 + \eta_{eff}\bar{E}_S\bar{E}_{LO}\left[\overline{\cos(2\pi \cdot (f_S - f_{LO}) \cdot t + \varphi_S)} + \underbrace{\overline{\cos(2\pi \cdot (f_S + f_{LO}) \cdot t + \varphi_S)}}_{=0}\right]$$
$$I_D(t) \propto \tfrac{1}{2}\bar{E}_S^2 + \tfrac{1}{2}\bar{E}_{LO}^2 + \eta_{eff}\bar{E}_S\bar{E}_{LO}\cos(2\pi \cdot (f_S - f_{LO}) \cdot t + \varphi_S)$$

with the efficiency η_{eff} of the optical mixing, which describes the efficiency of the matching of the spatial interference of the atmospheric signal beam and the LO beam (called "mode matching") and their temporal correlation. The efficiency η_{eff} is 1 for coherent beams, which are perfectly correlated in the spatial and temporal domain, whereas it approaches zero for non-coherent signals. In the case of

non-coherent radiation sources, e.g., solar background light, the signal $E_s(t)$ consists of a large number of oscillating waves with a random phase distribution φ_S. Thus the temporal average over the first cos-function (second equation above) would approach zero and the information about the difference frequency $f_S - f_{LO}$ would be lost. This makes the coherent detection method almost insensitive to non-coherent background light.

Due to the temporal averaging of the detector, only the difference frequency $f_S - f_{LO}$ is perceived, as the time average of the second cos-function with the sum frequency $f_S + f_{LO}$ signal is zero (second equation above, last term). The difference frequency is called the beat frequency f_{beat} and is a direct measure of the Doppler frequency shift and can be obtained using heterodyne ($f_{LO} \neq f_0$) or homodyne ($f_{LO} = f_0$) detection:

$$f_{\text{beat,heterodyne}} = |f_S - f_{LO}| = |f_0 + \Delta f - f_{LO}|$$
$$f_{\text{beat,heterodyne}} = |\Delta f|$$

The beat frequency f_{beat} provides only the absolute value of the frequency difference. It cannot be decided which frequency f_S or f_{LO} is higher or lower. For *heterodyne detection*, the frequency f_{LO} is selected such that it is different from the frequency of the outgoing laser pulse by a constant offset ($f_0 - f_{LO}$). Then the Doppler shift frequency Δf, with its positive and negative sign, is spread around this offset frequency, which allows determination of the sign and magnitude of the Doppler shift. In the case of *homodyne detection*, where $f_{LO} = f_0$, it is not possible to determine the sign of the Doppler shift.

The principle optical layout of a heterodyne detection DWL is shown in Fig. 30.2, where the frequency of the emitted laser pulse f_0 is monitored by a further heterodyne optical path with a reference detector. This allows for correcting the temporal variation of the emitted laser pulse frequency f_0. In addition, an optical beam steering device ("scanner") is included to deflect the outgoing laser pulse towards different LOS directions for the measurement of several wind components. The detector current $I_D(t)$ is digitized by an analog-to-digital converter and used to estimate the beat frequency $f_0 - \Delta f - f_{Lo}$. Several frequency estimators can be applied either in the time domain or after transforming the temporal signal by a Fourier transformation in the frequency domain.

In contrast to Doppler radar, where a fixed relation exists between the phase of successive radar pulses, this is not the case for laser pulses, which are generated by independent amplification processes within the laser. In addition, the backscattering particles in the atmosphere are randomly distributed and are not stationary but obey a thermal motion. This results in a randomly fluctuating phase $\varphi_{s,i}(t)$ from different scattering particles i for different times t, which causes a spatial and temporal variation of the signal called the *speckle" effect*. Thus it is not possible to average the time signal $I_D(t)$ of successive laser pulse returns for a coherent detection lidar, as is usually done for other lidar types. A temporal averaging of $I_D(t)$ would result in the loss of the phase information and thus in a loss of the

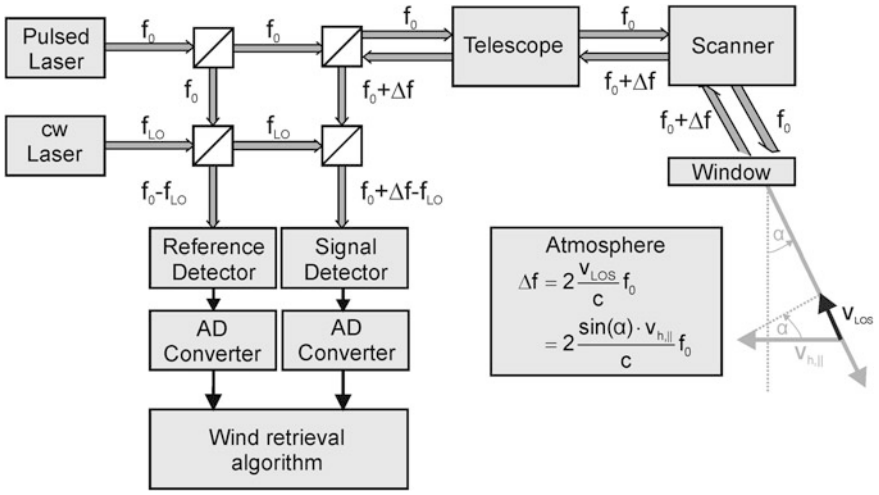

Fig. 30.2 Concept for a coherent, heterodyne DWL with optical mixing of cw laser with f_{LO} and emitted laser pulse with f_0 on the reference detector and Doppler shifted $f_0 + \Delta f$ atmospheric backscatter return on the signal detector; analog–digital (AD) converters provide digital signal; the laser pulses are transmitted through a telescope, scanner, and window to the atmosphere; the scanner is used to deflect the beam in the LOS direction and the v_{LOS} component is determined by the off-nadir angle α and component of the horizontal wind speed $V_{H,II}$ in the plane of the LOS vector

frequency information. The averaging of the signals of several laser pulse returns has to be done in the frequency domain. Several techniques for wind retrieval from coherent Doppler lidar signals are discussed by Smalikho (2003).

Coherent detection is limited to the narrow bandwidth of aerosol backscatter. Thus longer wavelengths in the infrared spectral region are preferred due to the availability of appropriate laser sources for eye-safety reasons and to minimize the broad bandwidth molecular backscatter and solar background. First coherent DWL were developed using gas lasers with CO_2 as active medium, which emit wavelengths of 10.6 μm, and applied to the detection of aircraft wake vortices by Huffaker et al. (1970). DLR activities started in the 1980s with cw-CO_2 lasers (Köpp et al. 1984). Today, solid-state lasers operating at 2.02 μm or fiber lasers with wavelengths of 1.5–1.6 μm are common sources for coherent DWL. The first airborne Doppler lidar measurements were made on board aircraft in the 1980s and were pointed sidewards (Bilbro et al. 1984) or in the flight-direction. Airborne Doppler lidars with conical scanning technique were developed at DLR in the 1990s using cw lasers (Rahm 1995) as true airspeed sensors (Rahm 2001). A pulsed airborne Doppler lidar with a conically scanning technique was developed within the scope of the French-German project WIND (Wind Infrared Doppler Lidar, see Fig. 30.3 and Table 30.2) The WIND instrument was the first airborne Doppler lidar for atmospheric research in 1999 capable of retrieving wind profiles to the ground by using nadir conical scanning (Reitebuch et al. 2001; Werner et al. 2001);. Airborne DWL observations with WIND were used to

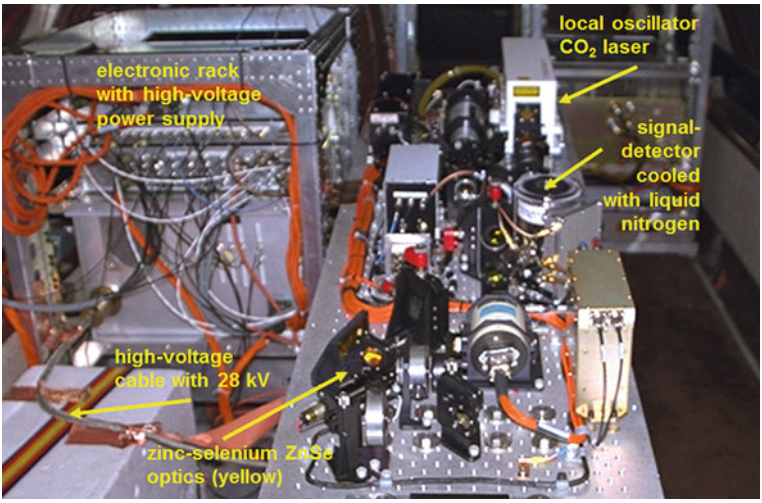

Fig. 30.3 Photo of the optical receiver of the 10.6 μm DWL WIND inside the Falcon aircraft with electronic rack and high-voltage supply for the CO_2 gas laser (*left*) and optical bench (*right*) with local oscillator CO_2 laser, signal detector with liquid nitrogen cooling, and optical elements made of zinc–selenium ZnSe; not visible are the telescope, scanning device and high-power, pulsed CO_2 laser

investigate the flow across the Alps (Reitebuch et al. 2003), the interaction between sea breeze and mistral winds (Drobinski et al. 2005; Bastin et al. 2006) and the *monsoon* flow in West Africa (Bou Karam et al. 2008; Drobinski et al. 2009). Based on the experience with WIND, a more compact airborne DWL was developed using a solid-state 2-μm laser (see Table 30.2). The 2-μm DWL was deployed during field campaigns in Europe for mesoscale studies (Weissmann et al. 2005a; Kiemle et al. 2011), in the North Atlantic for targeted observations (Weissmann et al. 2005b; Weissmann and Cardinali 2007), in Japan for typhoon targeting (Weissmann et al. 2012) and during the eruption of the *Eyjafjallajökull volcano* in 2010 (Schumann et al. 2011).

The detection and characterization of aircraft wake vortices was a major research application at DLR already in the mid-1980s using coherent DWLs with CO_2 lasers at 10.6 μm during several deployments at Frankfurt airport (Köpp 1994). By the end of the 1990s pulsed DWLs with fast scanning capability based on solid-state 2-μm lasers were used (Köpp et al. 2004) and wake vortex detection was demonstrated by DLR on board an aircraft (Rahm et al. 2007; Rahm and Smalikho 2008). Coherent DWLs were used at IPA for deriving turbulent quantities (Banakh et al. 1999; Smalikho et al. 2005), and to estimate turbulent fluxes in combination with trace-gas lidars (Giez et al. 1999; Kiemle et al. 2007; Kiemle et al. 2011) or turbulent flows around wind turbines (Käsler et al. 2010).

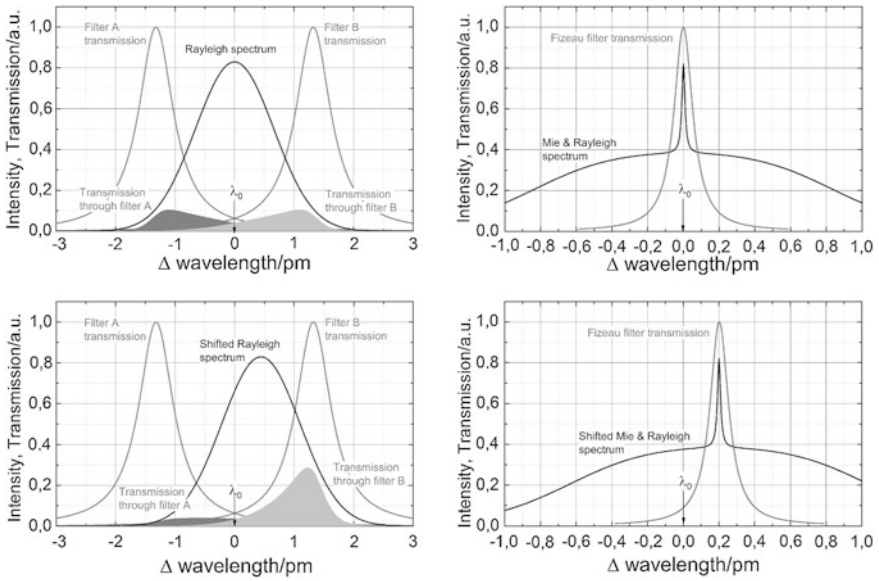

Fig. 30.4 Principle of direct-detection DWL with double-edge technique (*left*) and fringe-imaging technique (*right*) used for the ALADIN airborne demonstrator A2D and the space-borne lidar mission ADM-Aeolus; Rayleigh spectrum from molecular backscatter and double-edge filter A and B transmission (*left*) and additional Mie spectrum from aerosol backscatter and Fizeau filter transmission (*right*) for zero LOS speed (*top*) and Doppler shifted spectrum (*bottom*) for a wavelength of 355 nm; note the different wavelength scales on the left and right figures. The different signal levels transmitted through filter A and B (*left*, *grey areas*) are used to determine the Doppler shift from molecules; the transmitted signal at different spatial locations of the Fizeau filter transmission is used to determine the Doppler shift from aerosols (*right*)

30.3.2 Direct-Detection Doppler Wind Lidar

Compared to coherent DWL, where heterodyne detection by optical mixing is used as the principle, the direct-detection approach uses optical bandpass filters or alternatively an interferometer as spectral analyzer. The direct-detection DWL approach is mainly applied for using the broad bandwidth Rayleigh backscatter return from molecules, although it can also be applied to narrow bandwidth aerosol return. The principle of wind measurement with direct-detection Doppler lidar was first described and realized by Benedetti-Michelangeli et al. (1972) with a frequency-stabilized Ar-ion laser emitting at 488 nm and a spherical *Fabry–Perot interferometer* as spectral analyzer.

30.3.2.1 Filter Technique

The filter method is described using a common approach called the double-edge technique, which is also to be used for the future European space-borne DWL on the *Atmospheric Dynamics Mission* ADM-Aeolus. The double-edge technique uses

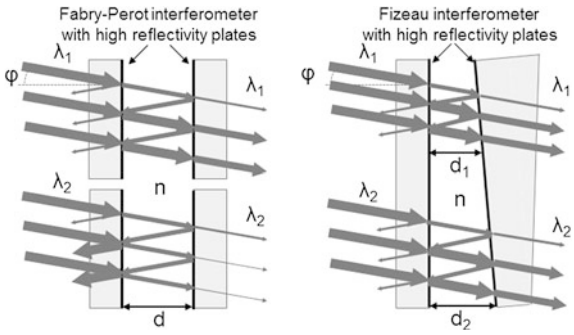

Fig. 30.5 Principle of a plane Fabry–Perot interferometer with distance d (*left*) and a Fizeau interferometer with distance d_1 (*upper part*) and d_2 (*lower part*) of the etalon (*right*) with two highly reflecting plates forming the etalon (refractive index n) and optical beams (*arrows*) for two different wavelengths λ_1 and λ_2; the thickness of the beams indicates their intensity; λ_1 fulfills the criteria for constructive interference for the Fabry–Perot interferometer ($\lambda_1 = 2{\cdot}d{\cdot}n{\cdot}\cos(\varphi)/k$) and for the upper part of the Fizeau interferometer ($\lambda_1 = 2{\cdot}d_1{\cdot}n{\cdot}\cos(\varphi)/k$) and is thus transmitted; λ_2 does not fulfill the interference criteria for the Fabry–Perot interferometer and is thus reflected, while it is transmitted in the lower part of the Fizeau interferometer ($\lambda_2 = 2{\cdot}d_2{\cdot}n{\cdot}\cos(\varphi)/k$)

two bandpass filters which are placed symmetrically around the maximum of the molecular spectral line with their maximum filter transmission at the edges of the line around the inflexion point (Fig. 30.4, left). The transmitted signal through each of these filters is detected, which is proportional to the convolution of the spectral filter transmission and the backscattered line shape from the atmosphere. For the case that both filters A and B have equal transmission characteristic ($T_A(\lambda) = T_B(\lambda + \Delta\lambda_{A,B})$) and are symmetrically placed around the Rayleigh spectral line with a separation of $\Delta\lambda_{A,B}$, then both filters would measure the same signal $I_A = I_B$, for a zero LOS wind speed. In the case of a Doppler shift $\Delta\lambda$, the transmitted signal through one filter would be higher than through the second one (Fig. 30.4, left, bottom). The ratio or contrast of I_A and I_B is used as a measure for the Doppler shift and is called the response R:

$$R = \frac{I_A}{I_B} \text{ or } R = \frac{I_A - I_B}{I_A + I_B}$$
$$R = f(T_A(\lambda), T_B(\lambda), I_{RBS}(\lambda, \Delta\lambda, T, p))$$

The Doppler shift can be derived from the response if the correspondence between both is determined through a calibration procedure. This is necessary because the response R is not only dependent on the Doppler shift $\Delta\lambda$, but also on the actual Rayleigh-Brillouin line shape of the backscattered signal $I_{RBS}(\lambda,\Delta\lambda,T,p)$, and thus depends on atmospheric temperature T and pressure p, as well as on the filter transmissions $T_A(\lambda)$ and $T_B(\lambda)$. Exact knowledge of the actual filter transmissions of the instrument is more critical for wind retrieval than is

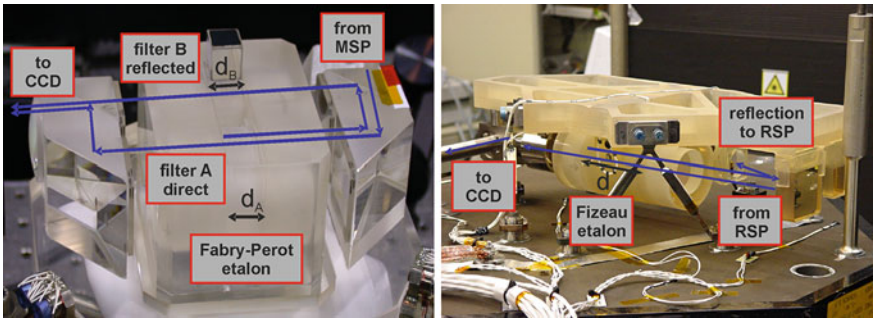

Fig. 30.6 Photo of the optical receiver of the ALADIN airborne demonstrator A2D with Rayleigh spectrometer (RSP, *left*) and its optical paths for filter A and B, and Mie spectrometer (MSP, *left*); optical beam paths towards the charge-coupled device (CCD) detector are indicated with *arrows*, the distances d_A and d_B of the Fabry–Perot etalons (*left*) and d of the Fizeau etalon (*right*) are indicated by double *arrows*

knowledge of sensitivity to the atmospheric temperature and pressure, which can be applied as a first-order correction to the retrieved wind speed.

Certainly the filter A and B bandwidths have to be smaller than the bandwidth of the molecular return signal (FWHM = 1.6 pm at 15 °C for a wavelength of 355 nm), which can be realized by a Fabry–Perot interferometer. As sketched in Fig. 30.5, a plane Fabry–Perot interferometer consists of two plane parallel optical plates (called the "etalon") with high reflectivity and separated by distance d (Vaughan et al. 1996). Multiple-beam interference of the incoming light leads to positive interference patterns (called fringes"), if the wavelength λ is a multiple k of the optical path $\lambda = 2 \cdot d \cdot n \cdot \cos(\varphi)/k$ (k: integer, n: refractive index, φ: incidence angle on plates).

When using a Fabry–Perot interferometer as a filter, then only the central ring ($\varphi = 0$) and not the complete, radial interference pattern is used. The two filters can be realized with the same Fabry–Perot interferometer, but with slightly different distances d_A and d_B at different parts of the Fabry–Perot interferometer (Fig. 30.6, left).

The double-edge technique was pioneered by Chanin et al. (1989) for stratospheric winds using the broadband molecular return with a laser wavelength of 532 nm, and for tropospheric winds using laser wavelengths of 1 064 nm and 532 nm for the narrow band aerosol return and 355 nm for the molecular return by Korb et al. (1992) and Gentry et al. (2000). The first airborne direct-detection Doppler lidar was developed by IPA and EADS-Astrium (Reitebuch et al. (2009), see Table 30.2 for key parameters, and Fig. 30.6) as the airborne prototype A2D (ALADIN airborne demonstrator) for the future space-borne instrument ALADIN (Atmospheric Laser Doppler Instrument) on the ADM-Aeolus mission of the European Space Agency ESA.

Another possibility to realize the filter technique is to use specific, very narrow-band molecular or atomic absorption lines. With absorption lines, only one filter

can be realized ("single edge technique"), which relies on the change in absolute intensity through this filter. The technique is limited to spectral regions where narrow bandwidth absorption lines are occurring at the emission wavelength of lasers. This is realized in the green spectral region at 532 nm and with iodine I_2 absorption lines. The use of the iodine molecular absorption lines as narrow-band filters for both molecular and aerosol backscatter at 532 nm was recently applied to measure sea-surface winds during the 2008 Olympic games in Beijing, China (Liu et al. 2008) and is also common for *high spectral resolution lidars* (HSRL, Esselborn et al. 2008).

30.3.2.2 Fringe Imaging Technique

Another implementation of the direct-detection DWL uses the spatial location of interference patterns ("fringes") and its displacement when a Doppler shift is present. This can be realized by a Fabry–Perot interferometer, where the movement of the radial-angular pattern of interference rings is used to determine the Doppler shift (Hirschberger and Ehret 2011). Another approach is based on a Fizeau interferometer, as for the satellite mission ADM-Aeolus and its airborne prototype A2D for determining the Doppler shift from the narrow bandwidth aerosol return (Fig. 30.6, right). A *Fizeau interferometer* also consists of an etalon, but opposed to a Fabry–Perot interferometer, where both etalon plates are plane-parallel with constant distance d, one of the plates is tilted by a small angle of several μrad. The resulting variation in distance d results in a distinct spatial location of an interference pattern where the condition for positive interference is fulfilled (Fig. 30.5, right). A Doppler shift of the signal will result in spatial displacement of the fringe, which is imaged onto a detector (Fig. 30.4, right). Therefore, a detector with several sensitive areas (e.g., a charge-coupled device CCD, as nowadays used in digital cameras) to provide pixel-wise discrete, spectral channels is needed for the fringe imaging technique.

30.4 Selected Results from Recent Airborne Wind Lidar Observations for Atmospheric Research

Two examples of airborne DWL observations during recent years are briefly discussed here to illustrate their potential for atmospheric research.

30.4.1 Monsoon Observations in West Africa

The monsoon is a seasonal atmospheric circulation induced by asymmetric heating of land and sea, which results in greater annual variation of temperature over large land areas compared with neighboring ocean surfaces. The monsoon onset is of great importance for Western Africa as it is linked to the start of the rain period. Here, the monsoon is a southerly, cool and humid flow and it was resolved on a large horizontal scale and vertically by airborne DWL observations during the

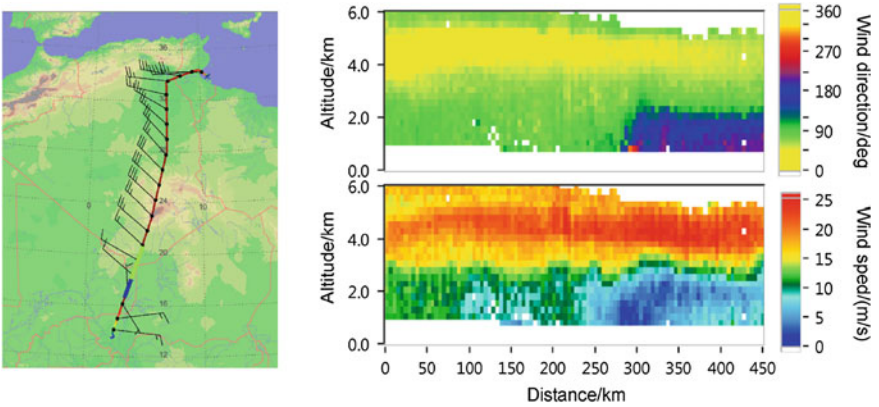

Fig. 30.7 Horizontal wind vector observations up to 6 km altitude above sea level with wind direction (*top*) and wind speed (*bottom*) from the Falcon aircraft from 20.6°N/4.7°E (0 km) to 16.8°N/3.3°E (450 km) on a flight from Djerba (Tunisia) to Niamey (Niger) on 30 June 2006 during the African Monsoon Multidisciplinary Analysis (AMMA) field campaign in West Africa; the Falcon flight track and the horizontal wind vector in flight altitude are shown (*left*) and the location of the observations are indicated on the flight track; the wind direction shows the southerly monsoon flow up to 2 km altitude; the African easterly jet in 4–5 km altitude is visible with higher wind speeds up to 25 m/s; *white* colors indicated non-valid winds after quality control and terrain for low altitudes

African Monsoon Multidisciplinary Analysis (AMMA) field experiment in 2006. The Falcon aircraft flew from Djerba (Tunisia) to Niamey (Niger) on 30 June 2006, and northwesterly winds were observed at a flight altitude of 11 km by the insitu wind sensor (Fig. 30.7, left). The southerly monsoon flow up to 2 km is clearly visible in the wind direction observations from the DWL up to the so-called intertropical discontinuity, where it interacts with the northeasterly, dry wind, the so-called Harmattan (Fig. 30.7, right, top). Above the monsoon flow the dry African easterly jet (a subtropical jet with an easterly wind direction in the troposphere over Africa) is present as a layer of higher wind speeds up to 25 m/s around 4–5 km altitude with a northeasterly direction on this day (Fig. 30.7, right, bottom). Airborne DWL observations were performed for the first time in this region and used for numerous case studies of dynamic processes in combination with mesoscale models, e.g., Bou Karam et al. (2008) and Drobinski et al. (2009).

30.4.2 Targeted Observations in the North Atlantic with 2-μm Wind Lidar

Airborne DWL observations for the purpose of improving weather forecasts were performed over the North Atlantic Ocean in November 2003. The Falcon aircraft with the 2-μm DWL and a dropsonde unit was directed towards so-called sensitive

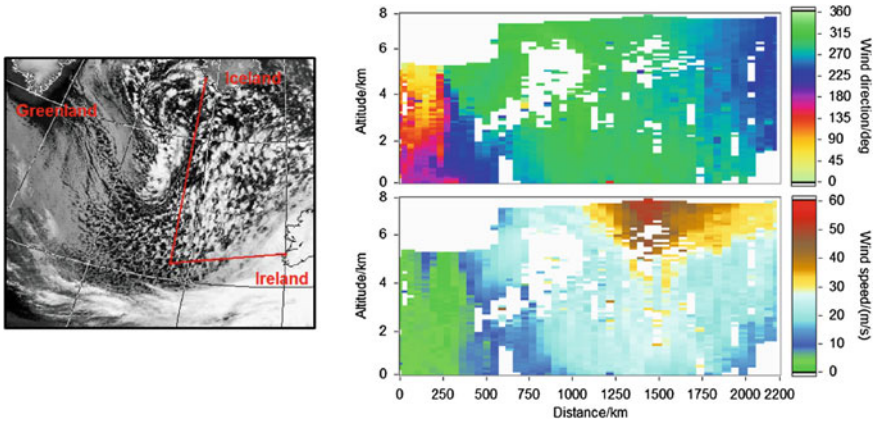

Fig. 30.8 2-μm DWL observations from a Falcon flight from Iceland to Ireland (*left*, superimposed on a visible satellite image) on 25 November 2003 during the Atlantic THORPEX Regional Campaign A-TReC (figure adapted from Weissmann et al. (2005b)); the observations are averaged over 40 km for horizontal wind direction (*top*) and wind speed (*bottom*); a high-altitude jet stream with wind speeds up to 67 m/s was targeted; location of the turning curve from north-south to west-east in the flight track is at a distance of 1 400 km; *white* colors indicate non-valid winds after quality control and different flight altitudes before and after 600 km distance

regions" where observations should be most beneficial for medium-range weather forecasts. These targeted lidar observations were assimilated into the numerical model of the *European Centre for Medium-Range Weather Forecasts* (ECMWF) and had a significant positive impact on the analysis and forecast results (Weissmann and Cardinali 2007). The wind observations from the lidar were averaged along the flight track to about 40 km in order to match the horizontal resolution of the lidar to the numerical model, which allows assigning a low representativeness error. An example is shown for the flight on 25 November 2003 from Iceland to Ireland (Fig. 30.8). Although the atmosphere is rather cloudy, the horizontal wind speed and direction could be derived without large gaps in coverage. The wind speed increased while flying from north to south up to 67 m/s while approaching a high-altitude jet stream. The instrumental error of the lidar observations could be quantified by a comparison with collocated wind measurements from dropsondes and resulted in a random error of 0.75–1.0 m/s (Weissmann et al. 2005b). The results from the impact studies with the assimilated DWL observations underlined the importance of additional wind observations, especially over the oceans, and demonstrated the potential of DWL. For the first time real DWL observations were assimilated into a global model and the findings support the high expectations for the future satellite DWL on ADM-Aeolus.

30.5 Outlook

Today, coherent DWLs with near-infrared wavelength (typically between 1.5–1.6 μm and 2 μm) are commercially available and routinely applied for assessing the wind energy potential and at some airports for wind profiling and wind shear detection. Research and development activities are focused towards further miniaturization for deployment of DWLs in wind turbines for gust detection or on airborne sensors for true-air speed, wake-vortex or *clear-air turbulence* detection. A space-borne direct-detection wind lidar will be deployed on the ADM-Aeolus mission in the near future as a technical demonstrator for future, operational wind lidars on *polar orbiting satellites* for global wind profiling.

References

Banakh, V.A., Smalikho, I.N., Köpp, F., Werner, C.: Measurements of turbulent energy dissipation rate with a CW Doppler lidar in the atmospheric boundary layer. J. Atmos. Oceanic Technol. **16**, 1044–1061 (1999). doi:10.1175/1520-0426(1999)016<1044:MOTEDR>2.0.CO;2

Bastin, S., Drobinski, P., Guenard, V., Caccia, J.-L., Campistron, B., Dabas, A., Delville, P., Reitebuch, O., Werner, C.: On the interaction between sea breeze and summer Mistral at the exit of the Rhone valley. Mon. Weather Rev. **134**, 1647–1668 (2006). doi:10.1175/MWR3116.1

Benedetti-Michelangeli, G., Congeduti, F., Fiocco, G.: Measurement of aerosol motion and wind velocity in the lower troposhere by Doppler optical radar. J. Atmos. Sci. **29**, 906–910 (1972). doi:10.1175/1520-0469(1972)029<0906:MOAMAW>2.0.CO;2

Bilbro, J., Fichtl, G., Fitzjarrald, D., Krause, M., Lee, R.: Airborne Doppler Lidar Wind Field Measurements. Bull. Am. Meteorol. Soc. **65**, 348–359 (1984). doi:10.1175/1520-0477(1984)065<0348:ADLWFM>2.0.CO;2

Bou Karam, D., Flamant, C., Knippertz, P., Reitebuch, O., Pelon, J., Chong, M., Dabas, A.: Dust emissions over Sahel associated with the West African monsoon inter-tropical discontinuity region: a representative case study. Quart. J. Roy. Meteorol. Soc. **134**, 621–634 (2008). doi:10.1002/QJ.244

Chanin, M.L., Garnier, A., Hauchecorne, A., Porteneuve, J.: A Doppler lidar for measuring winds in the middle atmosphere. Geophys. Res. Lett. **16**, 1273–1276 (1989). doi:10.1029/GL016i011p01273

Drobinski, P., Bastin, S., Guenard, V., Caccia, J.-L., Dabas, A.M., Delville, P., Protat, A., Reitebuch, O., Werner, C.: Summer Mistral at the exit of the Rhône valley. Quart. J. Roy. Meteorol. Soc. **131**, 353–375 (2005). doi:10.1256/qj.04.63

Drobinski, P., Bastin, S., Janicot, S., Bock, O., Dabas, A., Delville, P., Reitebuch, O., Sultan, B.: On the late northward propagation of the West African monsoon in summer 2006 in the region of Niger/Mali. J. Geophys. Res. **114**, D09108 (2009). doi:10.1029/2008JD011159

Esselborn, M., Wirth, M., Fix, A., Tesche, M., Ehret, G.: Airborne high spectral resolution lidar for measuring aerosol extinction and backscatter coefficients. Appl. Optics **47**, 346–358 (2008). doi:10.1364/AO.47.000346

Gentry, B.M., Chen, H., Li, S.X.: Wind measurements with 355-nm molecular Doppler lidar. Opt. Lett. **25**, 1231–1233 (2000). doi:10.1364/OL.25.001231

Giez, A., Ehret, G., Schwiesow, R., Davis, K.J., Lenschow, D.H.: Water Vapor Flux Measurements from ground-based vertically-pointed water vapor differential absorption and Doppler lidars. J. Atmos. Oceanic Technol. **16**, 237–250 (1999). doi:10.1175/1520-0426(1999)016<0237:WVFMFG>2.0.CO;2

Henderson, S.W., Gatt, P., Rees, D., Huffaker, R.M.: Wind lidar. In: Fujii, T., Fukuchi, T. (eds.) Laser Remote Sensing, pp. 469–722. Taylor & Francis Group, London (2005)

Hirschberger, M., Ehret, G.: Simulation and high-precision wavelength determination of noisy 2D Fabry–Pérot interferometric rings for direct-detection Doppler lidar and laser spectroscopy. Appl. Phys. B **103**, 207–222 (2011). doi:10.1007/s00340-011-4391-9

Huffaker, R.M., Jelalian, A.V., Thomson, J.A.: Laser-Doppler system for detection of aircraft trailing vortices. Proc. IEEE **58**, 322–326 (1970). doi:10.1109/PROC.1970.7636

Käsler, Y., Rahm, S., Simmet, R., Kühn, M.: Wake measurements of a multi-MW wind turbine with coherent long-range pulsed doppler wind lidar. J. Atmos. Oceanic Technol. **27**, 1529–1532 (2010). doi:10.1175/2010JTECHA1483.1

Kiemle, C., Brewer, W.A., Ehret, G., Hardesty, R.M., Fix, A., Senff, C., Wirth, M., Poberaj, G., LeMone, M.A.: Latent heat flux profiles from collocated airborne water vapor and wind lidars during IHOP_2002. J. Atmos. Oceanic Technol. **24**, 627–639 (2007). http://dx.doi.org/10.1175/JTECH1997.1

Kiemle, C., Wirth, M., Fix, A., Rahm, S., Corsmeier, U., Di Girolamo, P.: Latent heat flux measurements over complex terrain by airborne water vapour and wind lidars. Quart. J. R. Meteorol. Soc. **137**, 190–203 (2011). doi:10.1002/qj.757

Köpp, F., Schwiesow, R.L., Werner, C.: Remote measurements of boundary-layer wind profiles using a CW Doppler lidar. J. Clim. Appl. Meteorol. **23**, 148–154 (1984). doi:10.1175/1520-0450(1984)023<0148:RMOBLW>2.0.CO;2

Köpp, F.: Doppler lidar investigation of wake vortex transport between closely spaced parallel runways. AIAA J. **32**(4), 805–810 (1994). doi:10.2514/3.12057

Köpp, F., Rahm, S., Smalikho, I.: Characterization of aircraft wake vortices by 2-μm pulsed Doppler Lidar. J. Atmos. Oceanic Technol. **21**(2), 194–206 (2004). doi:10.1175/1520-0426(2004)021<0194:COAWVB>2.0.CO;2

Korb, C.L., Gentry, B.M., Weng, C.: The edge technique: theory and application to the lidar measurement of atmospheric winds. Appl. Optics **31**, 4202–4213 (1992). doi:10.1364/AO.31.004202

Liu, Z., Liu, B., Wu, S., Li, Z., Wang, Z.: High spatial and temporal resolution mobile incoherent Doppler lidar for sea surface wind measurements. Opt. Lett. **33**, 1485–1487 (2008). doi:10.1364/OL.33.001485

Rahm, S.: Measurement of a wind field with an airborne continuous-wave Doppler lidar. Opt. Lett. **20**, 216–218 (1995). doi:10.1364/OL.20.000216

Rahm, S.: Precursor experiment for an active true airspeed sensor. Opt. Lett. **26**, 319–321 (2001). doi:10.1364/OL.26.000319

Rahm, S., Smalikho, I., Köpp, F.: Characterization of aircraft wake vortices by airborne coherent Doppler lidar. J. Aircr. **44**, 799–805 (2007). doi:10.2514/1.24401

Rahm, S., Smalikho, I.: Aircraft wake vortex measurement with airborne coherent Doppler lidar. J. Aircr. **45**, 1148–1155 (2008). doi:10.2514/1.32896

Reitebuch, O., Werner, C., Leike, I., Delville, P., Flamant, P.H., Cress, A., Engelbart, D.: Experimental validation of wind profiling performed by the airborne 10 μm-heterodyne Doppler lidar WIND. J. Atmos. Oceanic Technol. **18**, 1331–1344 (2001). doi:10.1175/1520-0426(2001)018<1331:EVOWPP>2.0.CO;2

Reitebuch, O., Volkert, H., Werner, C., Dabas, A., Delville, P., Drobinski, P., Flamant, P.H., Richard, E.: Determination of air flow across the Alpine ridge by a combination of airborne Doppler lidar, routine radio-sounding and numerical simulation. Quart. J. Roy. Meteorol. Soc. **129**, 715–728 (2003). doi:10.1256/qj.02.42

Reitebuch, O., Lemmerz, C., Nagel, E., Paffrath, U., Durand, Y., Endemann, M., Fabre, F., Chaloupy, M.: The airborne demonstrator for the direct-detection Doppler wind lidar ALADIN on ADM-Aeolus. Part I: instrument design and comparison to satellite instrument. J. Atmos. Oceanic Technol. **26**, 2501–2515 (2009). doi:10.1175/2009JTECHA1309.1

Schumann, U., Weinzierl, B., Reitebuch, O., Schlager, H., Minikin, A., Forster, C., Baumann, R., Sailer, T., Graf, K., Mannstein, H., et al.: Airborne observations of the Eyjafjalla volcano ash

cloud over Europe during air space closure in April and May 2010. Atmos. Chem. Phys. **11**, 2245–2279 (2011). doi:10.5194/acp-11-2245-2011

Smalikho, I.: Techniques of wind vector estimation from data measured with a scanning coherent Doppler lidar. J. Atmos. Oceanic Technol. **20**, 276–291 (2003). doi:10.1175/1520-0426(2003)020<0276:TOWVEF>2.0.CO;2

Smalikho, I., Köpp, F., Rahm, S.: Measurement of atmospheric turbulence by 2-μm Doppler lidar. J. Atmos. Oceanic Technol. **22**(11), 1733–1747 (2005). doi:10.1175/JTECH1815.1

Vaughan, J.M., Steinvall, O., Werner, C., Flamant, P.H.: Coherent laser radar in Europe. Proc. IEEE **84**, 205–226 (1996). doi:10.1109/5.482229

Weissmann, M., Braun, F., Gantner, L., Mayr, G., Rahm, S., Reitebuch, O.: The Alpine mountain-plain circulation: airborne Doppler lidar measurements and numerical simulations. Mon. Weather Rev. **133**, 3095–3109 (2005a). http://dx.doi.org/10.1175/MWR3012.1

Weissmann, M., Busen, R., Dörnbrack, A., Rahm, S., Reitebuch, O.: Targeted observations with an airborne wind lidar. J. Atmos. Oceanic Technol. **22**, 1706–1719 (2005b). http://dx.doi.org/10.1175/JTECH1801.1

Weissmann, M., Cardinali, C.: Impact of airborne Doppler lidar observations on ECMWF forecasts. Quart. J. R. Meteorol. Soc. **133**, 107–116 (2007). doi:10.1002/qj.16

Weissmann, M., Langland, R.H., Cardinali, C., Rahm, S.: Influence of airborne Doppler wind lidar profiles near typhoon Sinlaku on ECMWF and NOGAPS forecasts. Quart. J. R. Meteorol. Soc. **138**, 118–130 (2012). doi:10.1002/qj.896

Werner, C., Flamant, P.H., Reitebuch, O., Köpp, F., Streicher, J., Rahm, S., Nagel, E., Klier, M., Herrmann, H., Loth, C., et al.: Wind infrared Doppler lidar instrument. Opt. Eng. **40**, 115–125 (2001). doi:10.1117/1.1335530

Werner, C.: Doppler wind lidar. In: Weitkamp, C. (ed.) Lidar—Range-Resolved Optical Remote Sensing of the Atmosphere, pp. 325–354. Springer, New York (2004)

Witschas, B., Vieitez, M.O., van Duijn, E.-J., Reitebuch, O., van de Water, W., Ubachs, W.: Spontaneous Rayleigh-Brillouin scattering of ultraviolet light in nitrogen, dry air, and moist air. Appl. Optics **49**, 4217–4227 (2010). doi:10.1364/AO.49.004217